

# STOCHASTIC REACHABILITY ANALYSIS FOR THE HYPERSONIC RE-ENTRY PROBLEM

**Amit Jain<sup>\*</sup>, Damien Guého<sup>†</sup>, Puneet Singla<sup>‡</sup>, Maruthi Akella<sup>§</sup>**

In this paper, a computationally efficient approach is presented to enable onboard computation of reachability sets for the hypersonic re-entry problem. The main idea is to consider the bounded control variables as random variables and represent the reachability sets as the level sets of the state probability density function. A main advantage of such an approach is that it provide not only the boundary of the reachability set but it also characterizes the probability distribution of state variable due to variation in control input. The computation of state density function due to variation in control input at each time is made tractable by computing desired order statistical moments of state density function at each time. Conjugate Unscented Transform (CUT) algorithm is used to compute the moment generating function. Finally, a prototype model of the hypersonic re-entry problem is considered to show the efficacy and utility of the proposed ideas.

## INTRODUCTION

Hypersonic flights are of utmost importance for mission involving flight to orbital or near orbital speeds above the atmosphere. The guidance and control of hypersonic flight present significant challenges in terms of onboard processing and accommodating uncertainties in control as well as state variables. Both safety and performance of hypersonic flight depend upon our ability to update trajectory and computing reachable flight envelope onboard the vehicle. The reachability flight envelope or set can be defined as the collection of all states which can be transversed from arbitrary initial condition due to the application of admissible control.

The computation of reachability sets has garnered a lot of attention in the context of the control of autonomous systems. Whether one is planning a path for a robotic system or designing a maneuver for a spacecraft to avoid a collision with another spacecraft, the calculation of optimal or feasible trajectories centered around the computation of reachability sets. Though one can obtain exact solution for reachability sets for linear time invariant systems, numerical approximations are necessary to compute the reachability sets for nonlinear systems. For certain classes of continuous dynamics, exact computation of the set of reachable states was shown by [1]. For more general classes of systems numerical approximations have been proposed in [2–7]. Alternately, the reachability questions are computed as zero-level set of the value function of an appropriate optimal control problem [8]. The computation of value function generally require the solution of the Hamilton-Jacobi-Bellman (HJB) or Issacs (HJI) equation. Various numerical tools such as sum-of-squares [9, 10] and Level

<sup>\*</sup>Graduate Student, Department of Aerospace Engineering, Pennsylvania State University, State College, PA-16802, Email: axj307@psu.edu

<sup>†</sup>Graduate Student, Department of Aerospace Engineering, Pennsylvania State University, State College, PA-16802, Email: djg76@psu.edu

<sup>‡</sup>Associate Professor, AIAA Associate Fellow, AAS Fellow, Department of Aerospace Engineering, Pennsylvania State University, State College, PA-16802, Email: psingla@psu.edu.

<sup>§</sup>Professor, AIAA Associate Fellow, AAS Fellow, Department of Aerospace Engineering, The University of Texas, Austin, TX, Email: makella@mail.utexas.edu

Set Methods [11] have been developed for reachable set computations [12–14]. Refs. [15, 16] have developed feedback controllers to generate largest time-limited backward reachable set while using the notion of occupation measure. Furthermore, ellipsoidal [17], support vector machine [18] and reason of interest approximation [19] are considered for reachability sets computations. While promising, all of these methods face a similar challenge with regards to computational scalability with the dimension of the system.

In this work, we take an alternative approach to compute the reachability sets in a computationally attractive manner. The main idea is to represent reachable sets as the level set of system state probability density function at a given instant of time. For this purpose, the admissible control set is assumed to be represented by a probability density function for control input at each time. By considering the response of each actuator as a random variable, a brute force evaluation of state density function for purposes of reachability characterization entails the combinatorial increase in number of samples over time. This is computationally intractable on most onboard implementations. Exploiting the fact that the control input at a specific time is independent of system states at that time, one can easily compute statistical moments associated with state density function. These finite order statistical moments represent the spectral content of the state density function and one can compute the state density function from computed moments by using various available tools such as Principle of maximum entropy [20] or sum of squares [21]. A main advantage of such an approach is that it provide not only the boundary of the reachability set but it also characterizes the probability distribution of state variable due to variation in control input.

The structure of paper is as follows: first, a brief introduction to reachability set problem is presented followed by the description of developed method. Finally, numerical simulation results are presented to show the efficacy of the proposed ideas.

## PROBLEM STATEMENT

Let us consider the problem of computation of reachability set for a generic nonlinear system in the following form:

$$\mathbf{x}_{k+1} = f(\mathbf{x}_k) + G(\mathbf{x}_k)h(\mathbf{u}_k) \quad (1)$$

where  $\mathbf{x}_k \in \mathbb{R}^n$  is the system state variable.  $\mathbf{u}_k \in \mathcal{U} \subset \mathbb{R}^m$  represents the control input variable at time instant  $t_k$ .  $\mathcal{U}$  is the set of admissible controls and is assumed to be described a density function  $p_{\mathbf{u}_k}(\mathbf{u}_k)$ . For example, a uniform density function can be used to represent the admissible control set,  $\mathcal{U}$  assumed to be a hypercube or a Gaussian density function can be used to represent an ellipsoidal admissible control set,  $\mathcal{U}$ . We define the reachability set for arbitrary initial state,  $\mathbf{x}_0$  as the set of all possible states at time  $t_N$  given  $\mathbf{u}_k \in \mathcal{U}$ . Mathematically, it can be written as:

$$\mathcal{R}(\mathbf{x}_0, \mathcal{U}, t_M) = \{\forall \mathbf{x} \in \mathbb{R}^n \mid \mathbf{u}_k \in \mathcal{U}, \forall k \in [0, M] \text{ s.t. } \mathbf{x}(t_M) = \mathbf{x}\}$$

As discussed in the previous section, the reachability analysis is a well-studied area. The main objective of this work is to develop a computationally efficient approach for the computation of reachability set for system described by Eq. (1) while exploiting recent advances in uncertainty propagation. The main idea of the presented approach is to consider the bounded control variables as random variables and represent the reachability sets by the state probability density function. However, such an approach require the sampling of control variable from admissible set at each time and number of samples increases exponentially over the number of time steps considered as illustrated in Figure (1). This is due to the fact that after first time step, one has to take all possible

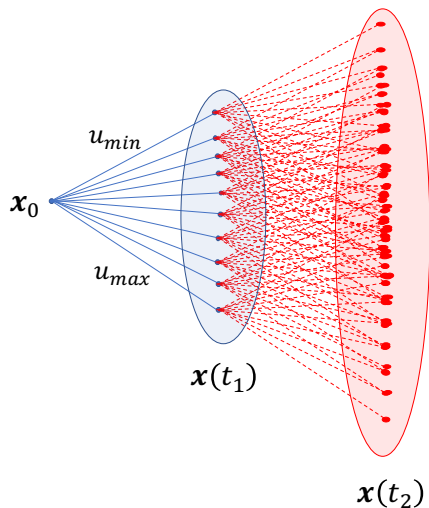


**Figure 1. Exponential Growth in Samples to Compute the Reachability Set.**

combinations of samples for  $\mathbf{x}_k$  and  $\mathbf{u}_k$ . For instance, if we take  $N_s$  samples of control variable at each time from admissible set  $\mathcal{U}$ , then one will have total  $N_s^M$  samples after  $M$  time steps. This is computationally intractable on most onboard implementations. In the next section, we discuss the developed approach, which avoid this exponential growth in number of samples for the computation of  $\mathcal{R}(\mathbf{x}_0, \mathcal{U}, t_M)$ .

### PROBABILISTIC REACHABILITY SET

To avoid the combinatorial growth of samples associated with computing reachability sets, we represent the state density function in terms of the finite number of statistical moments. Given the fact that characteristic function of a density function is Fourier transformation of a density function, computing the first few statistical moments of a density function are equivalent to computing Fourier coefficients of a periodic function. Since, the statistical moments behaves like Fourier coefficients, one can obtain better description of the state density function by computing higher order moments of  $\mathbf{x}_{k+1}$ . Furthermore, the state density function  $p_{\mathbf{x}_M}(\mathbf{x}_M)$  and hence the reachability set,  $\mathcal{R}(\mathbf{x}_0, \mathcal{U}, t_M)$  can then be obtained from propagated statistical moments by an application of the principle of maximum entropy (PME) [20].

To compute the desired order statistical moments in an efficient manner, we exploit the fact that the state variable  $\mathbf{x}_k$  at time  $t_k$  is independent of control input variable  $\mathbf{u}_k$  at time  $t_k$ . For the purpose of computing statistical moments, let us consider system equations in an index notation

$$x_{k+1}^\alpha = f^\alpha(\mathbf{x}_k) + G^{\alpha\beta}(\mathbf{x}_k) h^\beta(\mathbf{u}_k), \quad \alpha = 1, 2, \dots, n, \quad \beta = 1, 2, \dots, r \quad (2)$$

where  $x_{k+1}^\alpha$  and  $f^\alpha(\mathbf{x})$  represent the  $\alpha^{th}$  component of vectors  $\mathbf{x}_{k+1}$  and  $f(\mathbf{x}_k)$ , respectively. Similarly,  $G^{\alpha\beta}(\mathbf{x}_k)$  represents the  $\alpha\beta$  component of the matrix  $G(\mathbf{x}_k)$ . Notice that in index notation the repetition of the index corresponds to summation and hence

$$G^{\alpha\beta}(\mathbf{x}_k) h^\beta(\mathbf{u}_k) \equiv \sum_{\beta=1}^r G^{\alpha\beta}(\mathbf{x}_k) h^\beta(\mathbf{u}_k) \quad (3)$$

Now, the expected value of  $\mathbf{x}_{k+1}^\alpha$  can be written as:

$$\mathbb{E} [x_{k+1}^\alpha] = \mathbb{E} [f^\alpha (\mathbf{x}_k)] + \mathbb{E} [G^{\alpha\beta} (\mathbf{x}_k) h^\beta (\mathbf{u}_k)] \quad (4)$$

Making use of the fact that  $\mathbf{x}_k$  is an independent random vector from  $\mathbf{u}_k$ , the second term in the aforementioned equation can be written as:

$$\mathbb{E} [G^{\alpha\beta} (\mathbf{x}_k) h^\beta (\mathbf{u}_k)] = \mathbb{E} [G^{\alpha\beta} (\mathbf{x}_k)] \mathbb{E} [h^\beta (\mathbf{u}_k)] \quad (5)$$

Hence, the first order moment for state vector  $x_{k+1}$  can be written as:

$$\mathbb{E} [x_{k+1}^\alpha] = \mathbb{E} [f^\alpha (\mathbf{x}_k)] + \mathbb{E} [G^{\alpha\beta} (\mathbf{x}_k)] \mathbb{E} [h^\beta (\mathbf{u}_k)] \quad (6)$$

Since the density function for  $\mathbf{x}_k$  and  $\mathbf{u}_k$  is known and hence the first order moment for  $\mathbf{x}_{k+1}$  can be computed by separately sampling  $\mathbf{x}_k$  and  $\mathbf{u}_k$  space. Similarly, the second order moments can be computed as follows:

$$\begin{aligned} \mathbb{E} [x_{k+1}^\alpha x_{k+1}^\beta] &= \mathbb{E} \left[ (f^\alpha (\mathbf{x}_k) + G^{\alpha a} (\mathbf{x}_k) h^a (\mathbf{u}_k)) (f^\beta (\mathbf{x}_k) + G^{\beta b} (\mathbf{x}_k) h^b (\mathbf{u}_k)) \right] \quad (7) \\ &= \mathbb{E} [f^\alpha (\mathbf{x}_k) f^\beta (\mathbf{x}_k)] + \mathbb{E} [f^\alpha (\mathbf{x}_k) G^{\beta b} (\mathbf{x}_k) h^b (\mathbf{u}_k)] + \mathbb{E} [f^\beta (\mathbf{x}_k) G^{\alpha a} (\mathbf{x}_k) h^a (\mathbf{u}_k)] \\ &\quad + \mathbb{E} [G^{\alpha a} (\mathbf{x}_k) h^a (\mathbf{u}_k) G^{\beta b} (\mathbf{x}_k) h^b (\mathbf{u}_k)], \quad \alpha, \beta = 1, 2, \dots, n, \quad a, b = 1, 2, \dots, r \end{aligned} \quad (8)$$

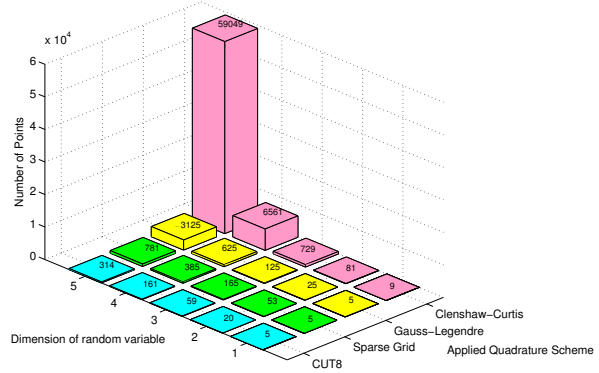
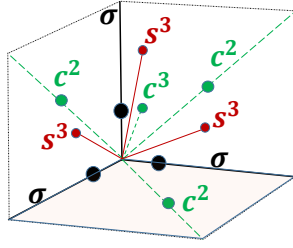
Once again, making use of the fact that  $\mathbf{x}_k$  is independent of  $\mathbf{u}_k$ , the aforementioned expression can be simplified as follows:

$$\begin{aligned} \mathbb{E} [x_{k+1}^\alpha x_{k+1}^\beta] &= \mathbb{E} [f^\alpha (\mathbf{x}_k) f^\beta (\mathbf{x}_k)] + \mathbb{E} [f^\alpha (\mathbf{x}_k) G^{\beta b} (\mathbf{x}_k)] \mathbb{E} [h^b (\mathbf{u}_k)] \\ &\quad + \mathbb{E} [f^\beta (\mathbf{x}_k) G^{\alpha a} (\mathbf{x}_k)] \mathbb{E} [h^a (\mathbf{u}_k)] + \mathbb{E} [G^{\alpha a} (\mathbf{x}_k) G^{\beta b} (\mathbf{x}_k)] \mathbb{E} [h^a (\mathbf{u}_k) h^b (\mathbf{u}_k)] \end{aligned} \quad (9)$$

Similarly, one can obtain the expressions for computing desired order statistical moments. For completion sake, we list the expression for third order moments in the Appendix. Furthermore, the state density function  $p_{\mathbf{x}_M}(\mathbf{x}_M)$  and hence the reachability set,  $\mathcal{R}(\mathbf{x}_0, \mathcal{U}, t_M)$  can then be obtained from propagated statistical moments by an application of the principle of maximum entropy (PME) [20].

### Computation of Statistical Moments

To compute the desired order moments for each module, one needs to sample the  $\mathbf{x}_k$  and  $\mathbf{u}_k$  spaces. The Monte Carlo (MC) methods traditionally used to evaluate statistical moments suffer from slow convergence rates. An efficient alternative to random sampling is the quadrature scheme, such as the Gaussian Quadrature that uses deterministic  $M^m$  sample points in  $m$  dimensions, chosen to reproduce  $2M - 1$  moments of the density function. For example, the number of points required to evaluate the expectation integral with only 5 points along each direction in a 6-dimensional space is  $5^6 = 15,625$ . Fortunately, the Gaussian quadrature rule is not minimal for  $m \geq 2$  [22], and there exists quadrature rules requiring fewer points in high dimensions [23]. For example, the Unscented



(a) Schematic of CUT Cubature Points in 3-D. (b) Comparison of number of  $8^{th}$  order quadrature points

**Figure 2 The Schematic of CUT points and growth of CUT points with number of random variables.**

Transformation (UT) is exact to degree 2 but with linear growth of points with dimension. However, the UT cannot be used to reproduce higher order moments.

In our prior work, a non-product quadrature rule known as the Conjugate Unscented Transformation (CUT) [24, 25] has been developed. The CUT approach can be considered an extension of the conventional UT method that satisfies additional higher order moment constraints. Rather than using tensor products as in Gauss quadrature, the CUT approach judiciously selects special structures to extract symmetric quadrature points constrained to lie on specially defined axes as shown in Figure (2(a)). These new sets of so-called sigma points are guaranteed to exactly evaluate expectation integrals involving polynomial functions with significantly fewer points. Figure (2(b)) represents the number of quadrature points required, for  $8^{th}$  order accuracy, by different quadrature schemes (CUT, Gauss-Legendre, Clenshaw-Curtis and Sparse Grid), for a uniform random variable, as a function of the dimensionality of the random variable. More details about the CUT methodology and its comparison with conventional quadrature rules can be found in Ref. [20, 24–31].

The following lists the CUT approximation of various expected values required for the computa-

tion of first two statistical moments:

$$\mathbb{E} [f^\alpha (\mathbf{x}_k)] = \sum_{i=1}^N w_x^i f^\alpha (\mathbf{x}_k^i), \quad \mathbb{E} [G^{\alpha\beta} (\mathbf{x}_k)] = \sum_{i=1}^N w_x^i G^{\alpha\beta} (\mathbf{x}_k^i) \quad (10)$$

$$\mathbb{E} [f^\alpha (\mathbf{x}_k) f^\beta (\mathbf{x}_k)] = \sum_{i=1}^N w_x^i f^\alpha (\mathbf{x}_k^i) f^\beta (\mathbf{x}_k^i) \quad (11)$$

$$\mathbb{E} [f^\alpha (\mathbf{x}_k) G^{\beta b} (\mathbf{x}_k)] = \sum_{i=1}^N w_x^i f^\alpha (\mathbf{x}_k^i) G^{\beta b} (\mathbf{x}_k^i) \quad (12)$$

$$\mathbb{E} [h^b (\mathbf{u}_k)] = \sum_{i=1}^N w_u^i h^b (\mathbf{u}_k^i) \quad (13)$$

$$\mathbb{E} [G^{\alpha a} (\mathbf{x}_k) G^{\beta b} (\mathbf{x}_k)] = \sum_{i=1}^N w_x^i G^{\alpha a} (\mathbf{x}_k^i) G^{\beta b} (\mathbf{x}_k^i) \quad (14)$$

$$\mathbb{E} [h^a (\mathbf{u}_k) h^b (\mathbf{u}_k)] = \sum_{i=1}^N w_u^i h^a (\mathbf{u}_k^i) h^b (\mathbf{u}_k^i) \quad (15)$$

where  $w_x^i$  and  $w_u^i$  corresponds to CUT points weight for density functions  $p_{\mathbf{x}_k}(\mathbf{x}_k)$  and  $p_{\mathbf{u}_k}(\mathbf{u}_k)$ , respectively. One can also compute expectation integrals appearing in the expressions for higher order moments through the application of CUT approach. After computing desired order statistical moments attach time, one can construct the state density function through the application of various density approximation tools such as PME or SOS. However, one needs to generate samples from newly approximated density function to compute statistical moments at next time step. Since CUT quadrature points are given for only Gaussian and uniform density functions, one can expand state variable at each time in terms of polynomial series of standardized Gaussian or uniform variable,  $\xi$

$$x_k^\alpha = \sum_{i=0}^N x_{k_i}^\alpha \phi_i(\xi) \Rightarrow \mathbf{x}_k = \mathbf{X}_{pc}(t) \Phi(\xi), \quad \alpha = 1, 2, \dots, n \quad (16)$$

where,  $\phi_k(\xi)$  are orthogonal polynomials associated with the assumed probability distribution for the input variables  $\xi$  (Hermite polynomials for normally distributed parameters, Legendre polynomials for uniform distribution, etc.) and can be computed through the application of the Gram-Schmidt orthogonalization process. Here  $\mathbf{X}$  are matrices composed of coefficients of the polynomial expansion for  $\mathbf{x}$ . Now, the known statistical moments of  $\mathbf{x}$  at a specific time step,  $k$ , can be written in terms of the unknown polynomial coefficients:

$$\mathbb{E} [x_k^\alpha] = x_{k_0}^\alpha, \quad \alpha = 1, 2, \dots, n \quad (17)$$

$$\mathbb{E} [x_k^\alpha x_k^\beta] = \sum_{i=1}^N x_{k_i}^\alpha x_{k_i}^\beta \mathbb{E} [\phi_i(\xi) \phi_i(\xi)], \quad \alpha, \beta = 1, 2, \dots, n \quad (18)$$

Note that the expected values of the product of the gPC basis functions,  $\mathbb{E} [\phi_k(\xi) \phi_k(\xi)]$ , are known from the properties of the functions. Depending on the order of the polynomial expansion, the desired moment constraints and the dimension of  $\mathbf{x}$ , the resulting equations can be over-determined, properly determined, or under-determined. In Ref. [32], an approach is presented to compute these

unknown polynomial series coefficients from desired order moment constraint equations. Now, one can generate an estimate of state density function of  $\mathbf{x}$  by substituting random samples of  $\xi$  in Eq. (16). Of course, there will be an improvement in accuracy when one goes to higher order PC coefficients and compute higher order moments. However, there is always a trade-off between the accuracy and the computational cost. Finally, the main steps of proposed approach can be enumerated as follows:

- Step 1: Generate CUT samples from standard Gaussian or Uniform random variables.
- Step 2: Compute CUT samples for state variables through the application of Eq. (16). If the state density function is assumed to be Gaussian or uniform, then only two of the coefficients will be non-zero.
- Step 3: Compute multi-dimensional expectation integrals while using Eq. (10)-Eq. (15) to compute desired order statistical moments for state variable of Eq. (6)-Eq. (9).
- Step 4: Recompute polynomial series coefficients through moment matching and go to Step 2.

## NUMERICAL RESULTS

In this section, we consider the hypersonic re-entry problem to assess the efficacy of the developed approach to compute the reachability set. We consider two different maneuvers for hypersonic re-entry problem. The first maneuver is adapted from Ref. [33] and corresponds to the space shuttle reentry with heating constraints. The second maneuver corresponds to maximum impact energy of the glide weapon at the target [34] and is of significant importance to the mission of conventional prompt global strike (CGPS). A low-fidelity flight dynamics model for both the maneuvers is given as:

$$\begin{aligned}
 \dot{h} &= v \sin \gamma \\
 \dot{v} &= -\frac{D(h, v, \alpha)}{m} - g(h) \sin \gamma \\
 \dot{\gamma} &= \frac{L(h, v, \alpha)}{mv} \cos \beta + \cos \gamma \left( \frac{v}{R_e + h} - \frac{g(h)}{v} \right) \\
 \dot{\theta} &= \frac{v}{R_e + h} \cos \gamma \sin \psi \sin \theta \\
 \dot{\psi} &= \frac{L(h, v, \alpha)}{mv \cos \gamma} \sin \beta + \frac{v}{R_e + h} \cos \gamma \sin \psi \sin \theta \\
 \dot{\phi} &= \frac{v}{R_e + h} \cos \gamma \sin \psi / \cos \theta
 \end{aligned} \tag{19}$$

where  $h$ ,  $v$  and  $\gamma$  represent the altitude, velocity, and flight-path angle of the vehicle.  $\theta$ ,  $\phi$  and  $\psi$  represent is latitude, longitude, and azimuth angles, respectively. The state vector  $\mathbf{x}$  is defined as follows:

$$\mathbf{x} = [h, v, \gamma, \theta, \psi, \phi]^T$$

The gravity,  $g(h)$ , atmospheric density,  $\rho(h)$ , lift,  $L$  and drag,  $D$  are computed according to the following models:

$$\begin{aligned}
g(h) &= \mu/(R_e + h)^2, \quad \rho(h) = \rho_0 \exp[-h/h_r] \\
L(h, v, \alpha) &= \frac{1}{2}c_L(\alpha)S\rho(h)v^2, \quad C_L(\alpha) = a_0 + a_1\alpha \\
D(h, v, \alpha) &= \frac{1}{2}c_D(\alpha)S\rho(h)v^2, \quad C_D(\alpha) = b_0 + b_1\alpha + b_2\alpha^2
\end{aligned} \tag{20}$$

The angle of attack  $\alpha$  and yaw angle  $\beta$  are considered to be control input variables. For reachability set computation, the continuous time model of Eq. (19) is discretized by making use of first order finite difference. The various terms of discretized model of Eq. (1) are given as follows:

$$f(\mathbf{x}_k) = \begin{bmatrix} h_k + v_k \sin \gamma_k dt \\ v_k - \frac{\mu}{(R_e + h_k)^2} \sin \gamma_k dt \\ \gamma_k + \cos \gamma_k \left( \frac{v_k}{R_e + h_k} - \frac{\mu}{(R_e + h_k)^2 v_k} \right) dt \\ \theta_k + \frac{v_k}{R_e + h_k} \cos \gamma_k \cos \psi_k dt \\ \psi_k + \frac{v_k}{R_e + h_k} \cos \gamma_k \sin \psi_k \sin \theta_k dt \\ \phi_k + \frac{v_k}{R_e + h_k} \cos \gamma_k \cos \theta_k \end{bmatrix} dt \tag{21}$$

$$G(\mathbf{x}_k) = \begin{bmatrix} 0 & 0 & 0 & 0 & 0 & 0 \\ 0 & -\frac{\rho_0}{2m} e^{-\frac{h_k}{h_r}} v_k^2 S dt & 0 & 0 & 0 & 0 \\ 0 & 0 & -\frac{\rho_0}{2m} e^{-\frac{h_k}{h_r}} v_k S dt & 0 & 0 & 0 \\ 0 & 0 & 0 & 0 & 0 & 0 \\ 0 & 0 & 0 & 0 & -\frac{\rho_0}{2m \cos \gamma_k} e^{-\frac{h_k}{h_r}} v_k S dt & 0 \\ 0 & 0 & 0 & 0 & 0 & 0 \end{bmatrix} \tag{22}$$

$$h(\mathbf{u}_k) = \begin{bmatrix} 0 \\ b_0 + b_1\alpha_k + b_2\alpha_k^2 \\ (a_0 + a_1\alpha_k) \cos \beta_k \\ 0 \\ (a_0 + a_1\alpha_k) \sin \beta_k \\ 0 \end{bmatrix} \tag{23}$$

For all simulations in this section, CUT-8 points are used to compute different expectation integrals of Eq. (6) and Eq. (9). At each time instant, the first two moments are used to approximate state density function as a Gaussian density function with computed mean and variance and new CUT points are sampled from this new Gaussian distribution.

### First Maneuver

The first maneuver is adapted from Ref. [33] and different simulation parameters are listed in Tables 1 and 2. The initial state vector is assumed to be a Gaussian random variable with

**Table 1. Parameters of the shuttle model equations**

$\mu(\text{ft}/\text{s}^2)$	$\rho_0(\text{lb}/\text{ft}^3)$	$R_e(\text{ft})$	$h_r(\text{ft})$	$S(\text{ft}^2)$	$m(\text{lb})$
$0.1407654 \times 10^{17}$	0.002378	20,902,900	23800	2690	6309.44

**Table 2. Lift and Drag Coefficients**

$a_0$	$a_1$	$b_0$	$b_1$	$b_2$
-0.20704	0.029244	0.07854	$-0.61592 \times 10^{-2}$	$0.621408 \times 10^{-3}$

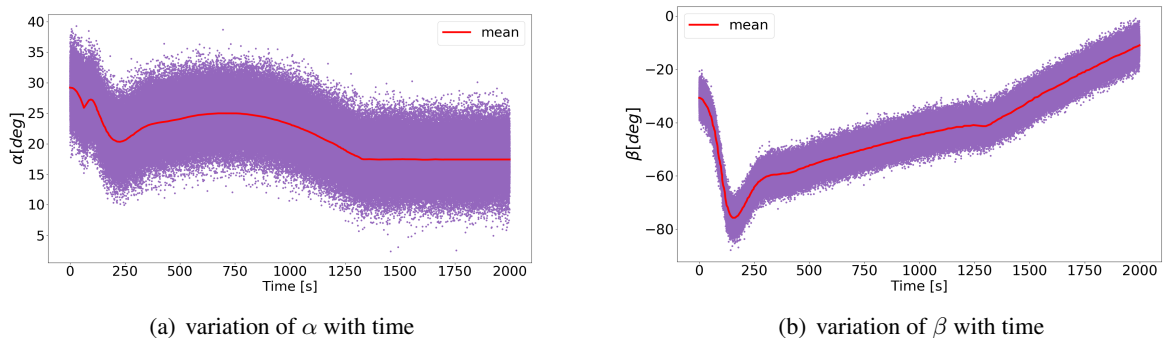
following mean and variance.

$$\mu_{\mathbf{x}_0} = [260,000 \text{ ft}, 25600 \text{ ft/s}, -1^\circ, 0, -1^\circ, 0]^T \quad (24)$$

$$\Sigma_{\mathbf{x}_0} = \begin{bmatrix} 3000^2 & 0 & 0 & 0 & 0 & 0 \\ 0 & 0 & 0 & 0 & 0 & 0 \\ 0 & 0 & 0 & 0 & 0 & 0 \\ 0 & 0 & 0 & (0.5^\circ)^2 & 0 & 0 \\ 0 & 0 & 0 & 0 & (0.5^\circ)^2 & 0 \\ 0 & 0 & 0 & 0 & 0 & 0 \end{bmatrix} \quad (25)$$

The admissible control set  $\mathcal{U}$  is defined by a Gaussian distribution with time varying mean defined by optimal control profile given in Ref. [33] with standard deviation of  $3^\circ$  for both  $\alpha$  and  $\beta$ . The mean control profile (red line) along with 10000 MC samples for control input variables are shown in Fig. 3. The mean control profile here corresponds to the optimal trajectory of the space shuttle reentry where the heating is constraint to be in safe limits to prevent the shuttle from burning.

The ground truth for reachability set is defined by taking 10,000 MC samples at initial time for state vector and 10,000 MC samples for control input vector at each time. The developed approach with CUT8 samples (745 for states and 21 for control) is used to compute mean and covariance of state vector at each time. Fig. 4 shows the mean (red color) with green colored  $3\sigma$  bounds for each state variable. The 10000 MC samples at each time are also superimposed in this figure with purple dots. Form this figure, it is clear that the MC samples lies within  $3\sigma$  bound and hence one can conclude that first two moments are good to compute the reachability set. Also, it can be observed

**Figure 3. Control inputs with Gaussian uncertainty for first maneuver**

that the general trend of altitude  $h$ , velocity  $v$  and azimuth  $\psi$  is decreasing and for latitude  $\theta$  & longitude  $\phi$ , is increasing. For the flight-path angle  $\gamma$ , the overall trend is decreasing but due to various humps occur on the way, its value oscillates locally.

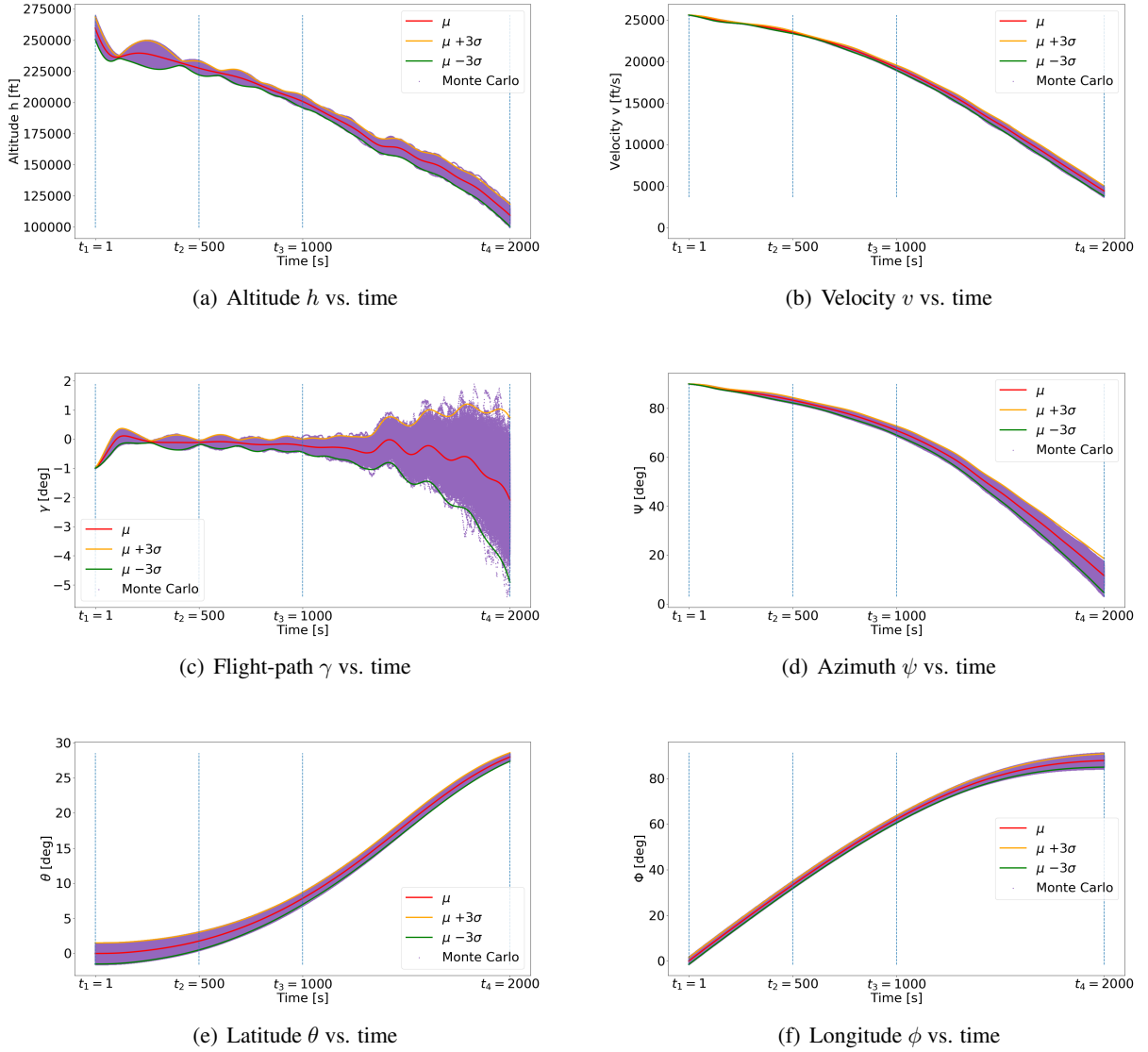


**Figure 4. Reachability analysis of states for first maneuver**

Fig. 5, Fig. 6 and Fig. 7 show the contour plots of various 2D projections of six dimensional state density function, i.e., reachability sets superimposed with MC runs at four different time intervals ( $t_1 = 1s$ ,  $t_2 = 500s$ ,  $t_3 = 1000s$  and  $t_4 = 2000s$ ). These plots once again confirm that the state density function can be approximated well with Gaussian density function for this particular maneuver case. Furthermore, the correlations between different variables depicted in contour plots of Fig. 5, Fig. 6 and Fig. 7 are in agreement with general behavior of trajectories in Fig. 4. For example, the positive correlation between  $h$  and  $v$  at time instants  $t_1$ ,  $t_3$  and  $t_4$  can be explained due to increase in spread around mean for  $h$  and  $v$  as shown in Fig. 4(a) and Fig. 4(b) at those

time instants. Similarly, the negative correlation between  $h$  and  $\theta$  at time instants  $t_3$  and  $t_4$  can be explained due to increase in spread around mean value of  $h$  with decrease in spread around mean value of  $\theta$  at these time instants in Fig. 4(a) and Fig. 4(e).

Finally, one can observe that the variation in optimal control profile results in  $2^\circ$  and  $8^\circ$  spread around mean values for latitude and longitude respectively at the end of the maneuver.

## Second Maneuver

The Second maneuver is adapted from Ref. [34] and the simulation parameter values are listed in Tables 3 and 4.

**Table 3. Parameters of the glider model equations**

$\mu(\text{m}^3/\text{s}^2)$	$\rho_0(\text{kg}/\text{m}^3)$	$R_e(\text{m})$	$h_r(\text{m})$	$S(\text{m}^2)$	$m(\text{kg})$
$3.986 \times 10^{14}$	1.2	$6.378 \times 10^6$	7500	0.30	340

**Table 4. Lift and Drag Coefficients**

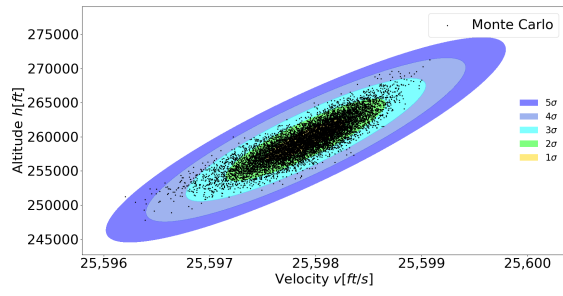
$a_0$	$a_1$	$b_0$	$b_1$	$b_2$
0	1.6	0.06	0	1.7

The initial state here is also assumed to be Gaussian with mean and variance as,

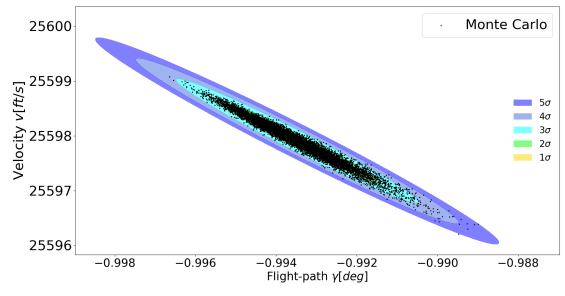
$$\mu_{\mathbf{x}_0} = [80000m, 5000m/s, -35.0822^\circ, 0, 0, 0]^T \quad (26)$$

$$\Sigma_{\mathbf{x}_0} = \begin{bmatrix} 1^2 & 0 & 0 & 0 & 0 & 0 \\ 0 & 0 & 0 & 0 & 0 & 0 \\ 0 & 0 & 0 & 0 & 0 & 0 \\ 0 & 0 & 0 & (0.5^\circ)^2 & 0 & 0 \\ 0 & 0 & 0 & 0 & (0.5^\circ)^2 & 0 \\ 0 & 0 & 0 & 0 & 0 & 0 \end{bmatrix} \quad (27)$$

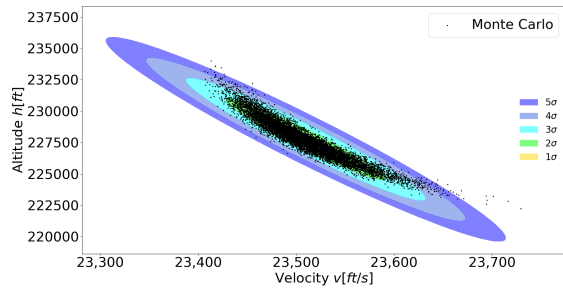
For control, the time varying mean is taken as the optimal profile of the  $\alpha$  and  $\beta$  as given in Ref. [34] with a standard deviation of  $3^\circ$  in both. The mean control profile (red line) along with 10000 MC samples for control input variables are shown in Fig. 8. The mean control profile here corresponds to maximum impact energy of the glide weapon at the target. These types of weapons are of significant importance to the mission of conventional prompt global strike (CGPS) [35]. The ground truth for reachability set is defined by taking 10,000 MC samples at initial time for state vector and 10,000 MC samples for control input vector at each time. The developed approach with CUT8 samples (745 for states and 21 for control) is used to compute mean and covariance of state vector at each time. Fig. 9 shows the mean (red color) with green colored  $3\sigma$  bounds for each state variable. The 10000 MC samples at each time are also superimposed in this figure with purple dots. From this figure, it is clear that the MC samples lies within  $3\sigma$  bound and hence one can conclude that first two moments are good to compute the reachability set. Also, observe that the general trend of altitude  $h$  & velocity  $v$  is decreasing and for azimuth  $\psi$  & longitude  $\phi$  is increasing. For the flight-path angle  $\gamma$  & latitude  $\theta$ , the values first increases and then after some point of time decreases.



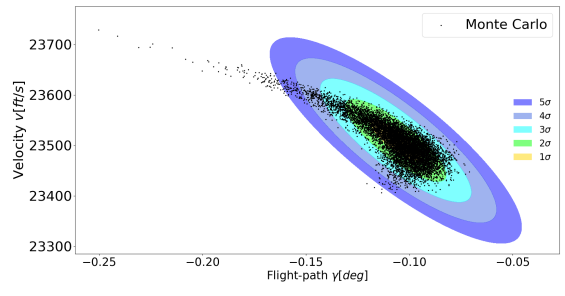
(a)  $h$  vs.  $v$  at time  $t_1$



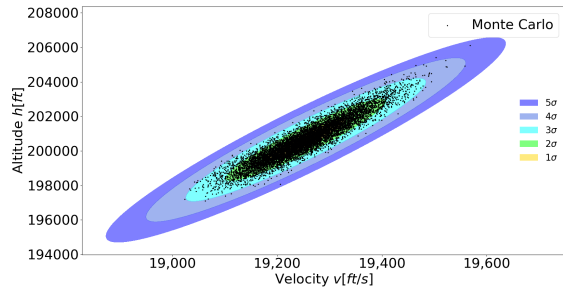
(b)  $v$  vs.  $\gamma$  at time  $t_1$



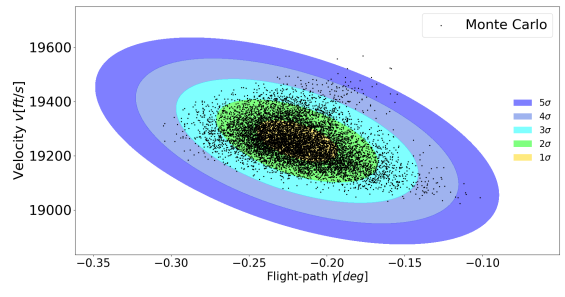
(c)  $h$  vs.  $v$  at time  $t_2$



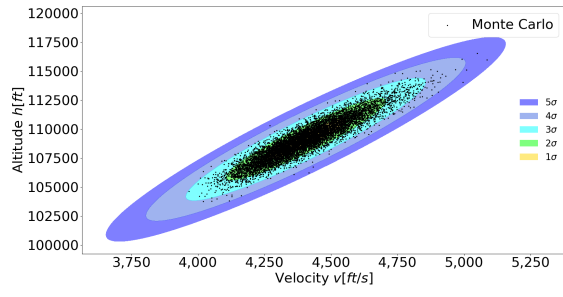
(d)  $v$  vs.  $\gamma$  at time  $t_2$



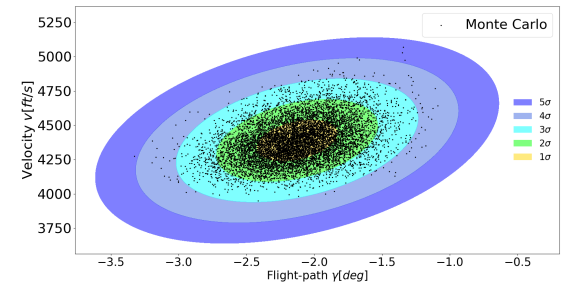
(e)  $h$  vs.  $v$  at time  $t_3$



(f)  $v$  vs.  $\gamma$  at time  $t_3$



(g)  $h$  vs.  $v$  at time  $t_4$



(h)  $v$  vs.  $\gamma$  at time  $t_4$

**Figure 5. Variation of altitude vs. velocity & velocity vs. flight-path at different time-steps**

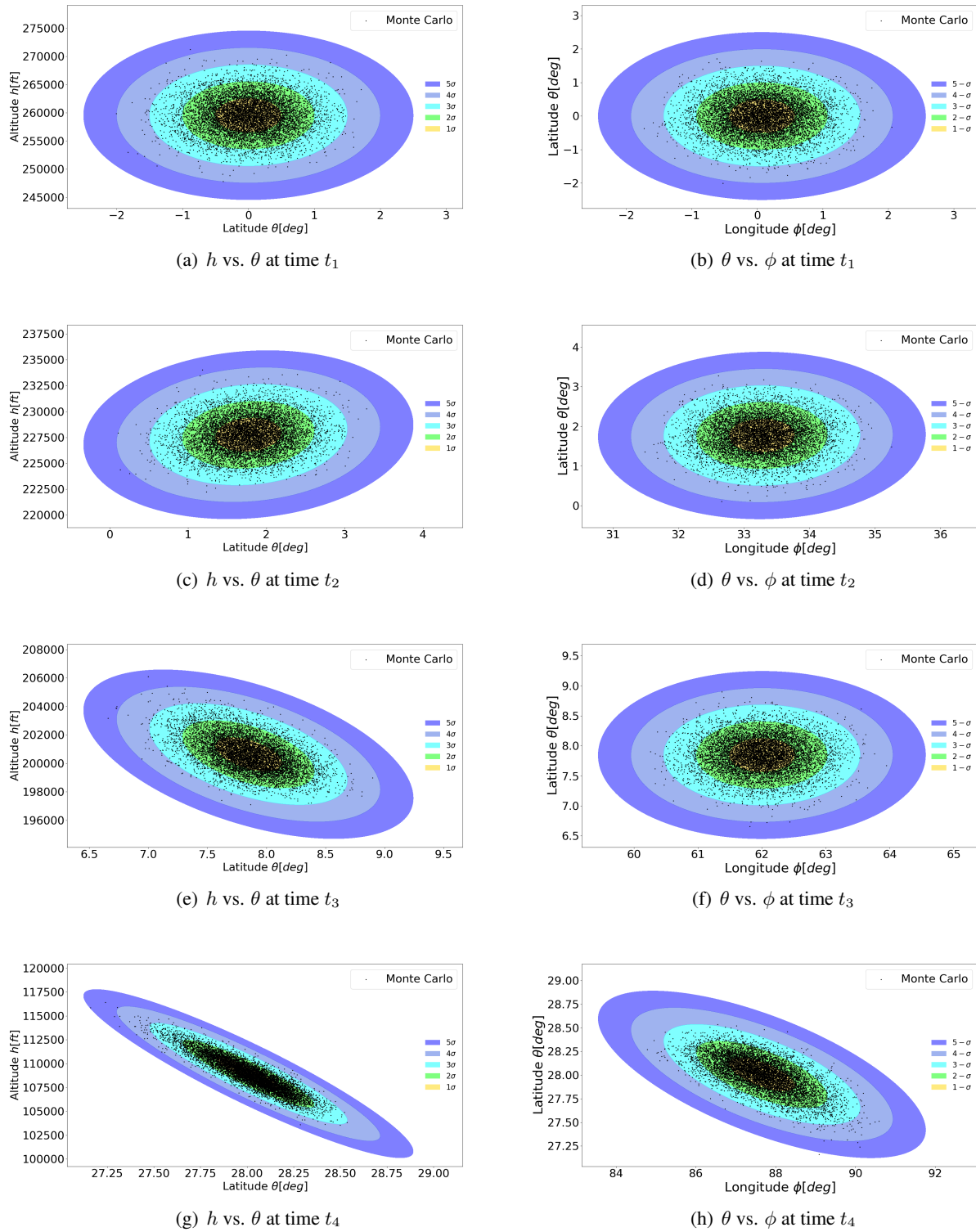
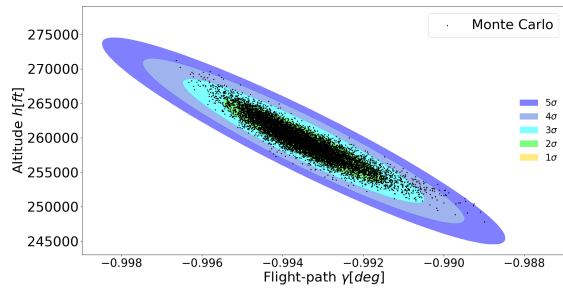
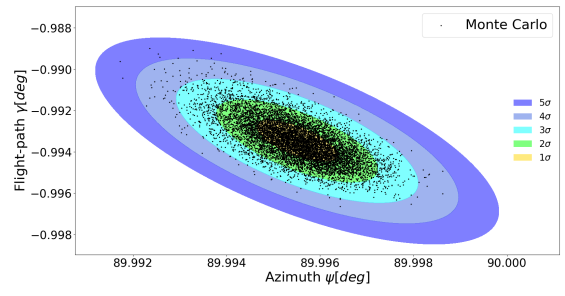


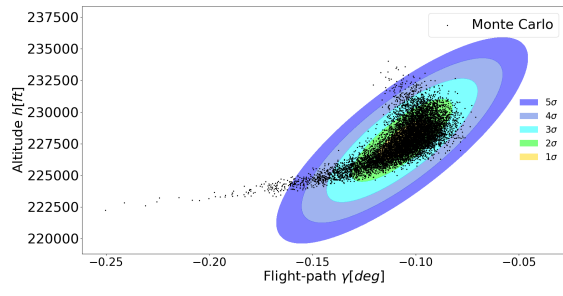
**Figure 6. Variation of altitude vs. latitude & latitude vs. longitude at different time-steps**



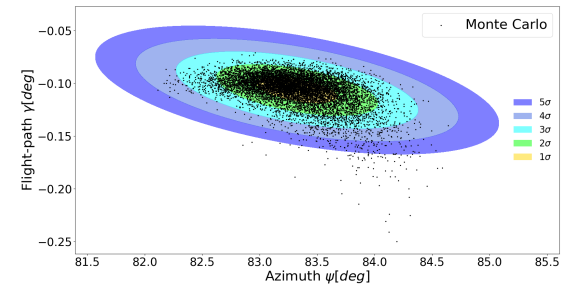
(a)  $h$  vs.  $\gamma$  at time  $t_1$



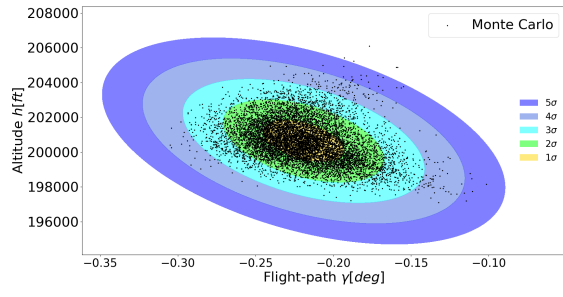
(b)  $\gamma$  vs.  $\psi$  at time  $t_1$



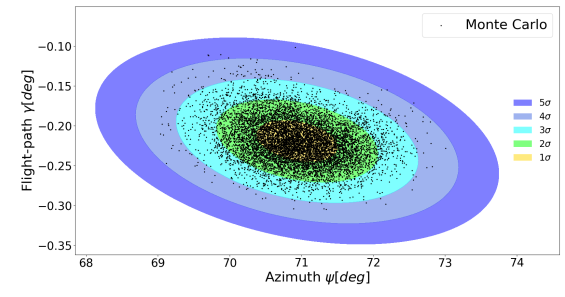
(c)  $h$  vs.  $\gamma$  at time  $t_2$



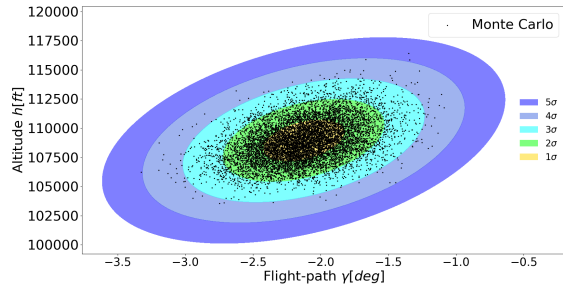
(d)  $\gamma$  vs.  $\psi$  at time  $t_2$



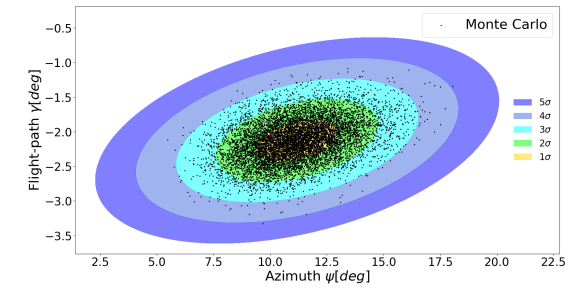
(e)  $h$  vs.  $\gamma$  at time  $t_3$



(f)  $\gamma$  vs.  $\psi$  at time  $t_3$

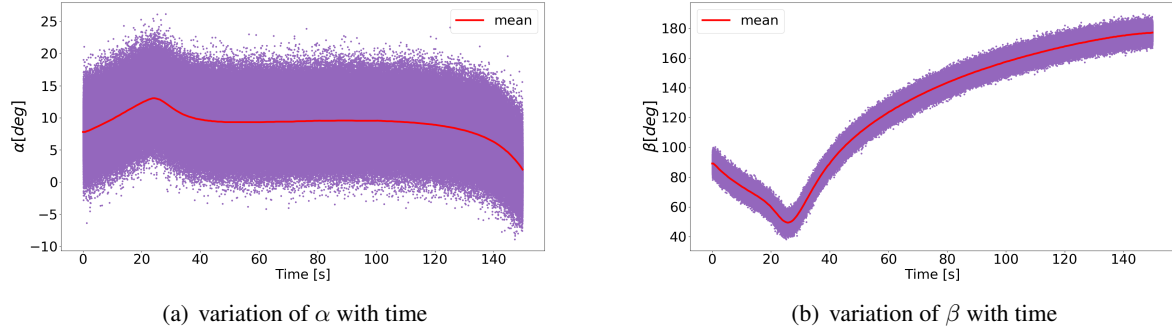


(g)  $h$  vs.  $\gamma$  at time  $t_4$



(h)  $\gamma$  vs.  $\psi$  at time  $t_4$

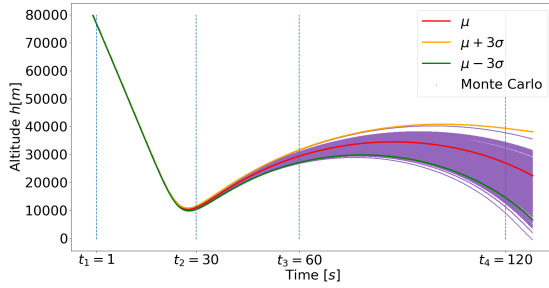
**Figure 7. Variation of altitude vs. flight-path & flight-path vs. azimuth at different time-steps**



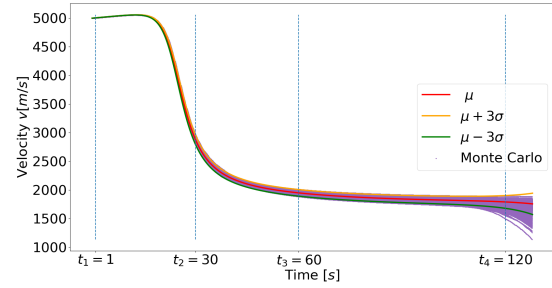
**Figure 8. Control inputs with Gaussian uncertainty for second maneuver**

Fig. 10, Fig. 11 and Fig. 12 show the contour plots of various 2D projections of six dimensional state density function, i.e., reachability set superimposed with MC runs at four different time intervals ( $t_1 = 1s$ ,  $t_2 = 30s$ ,  $t_3 = 60s$  and  $t_4 = 120s$ ). These plots once again confirm the approximation of state density function with Gaussian density function. For example, the positive correlation between  $h$  and  $\gamma$  at  $t_2$ ,  $t_3$  and  $t_4$  in Fig. 12 can be explained due to increase in spread around mean for  $h$  and  $\gamma$  as shown in Fig. 4(a) and Fig. 4(c) at those time instants.

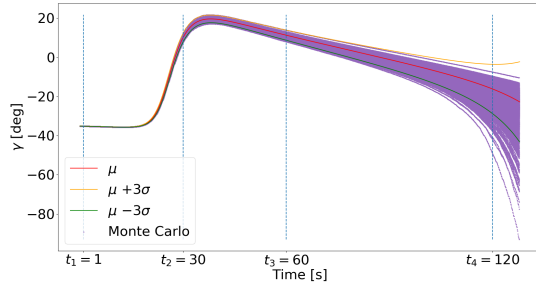
Finally, one can observe that the variation in optimal control profile results in about  $3000m$ ,  $3^\circ$  and  $3^\circ$  spread around mean values for altitude, latitude and longitude respectively at time  $t_4$ .



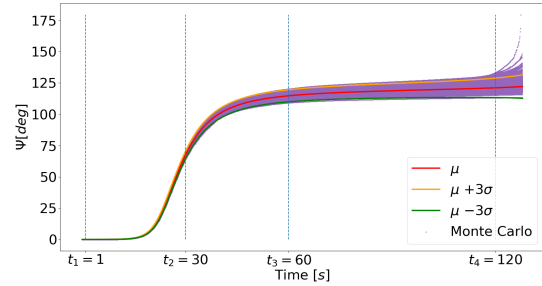
(a) Altitude  $h$  vs. time



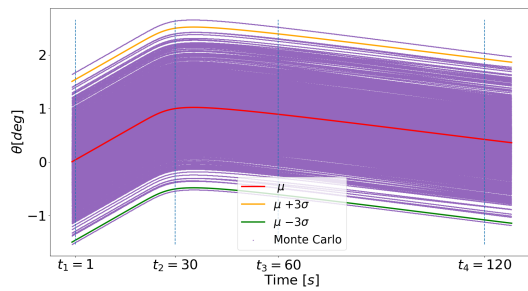
(b) Velocity  $v$  vs. time



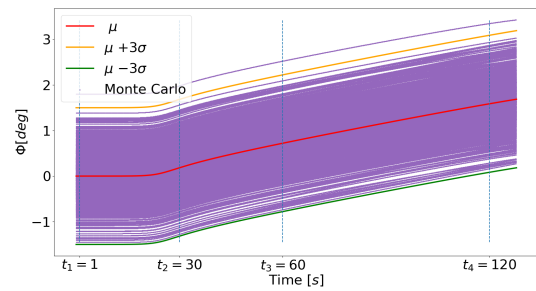
(c) Flight-path  $\gamma$  vs. time



(d) Azimuth  $\psi$  vs. time

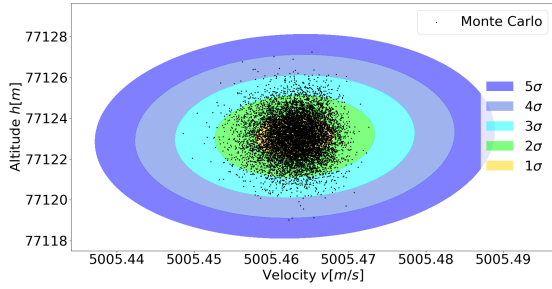


(e) Latitude  $\theta$  vs. time

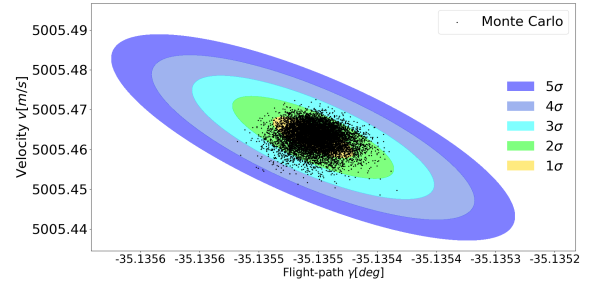


(f) Longitude  $\phi$  vs. time

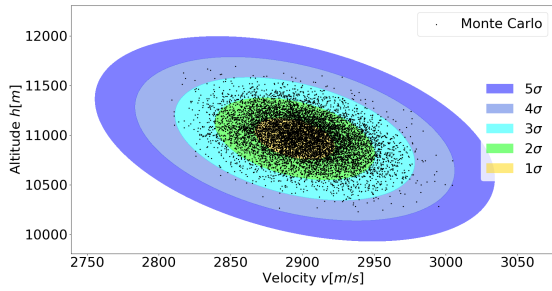
**Figure 9. Reachability analysis of states for second maneuver**



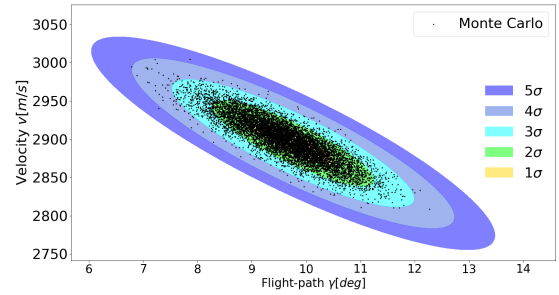
(a)  $h$  vs.  $v$  at time  $t_1$



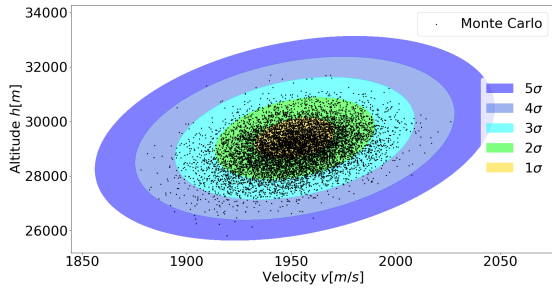
(b)  $v$  vs.  $\gamma$  at time  $t_1$



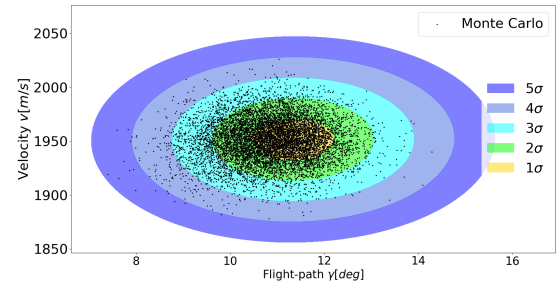
(c)  $h$  vs.  $v$  at time  $t_2$



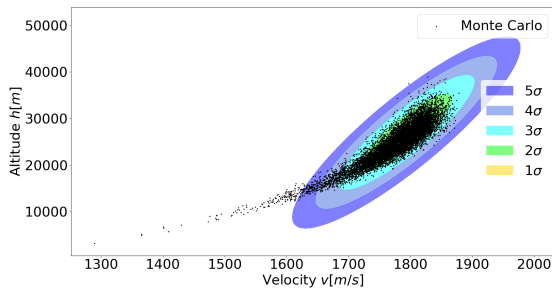
(d)  $v$  vs.  $\gamma$  at time  $t_2$



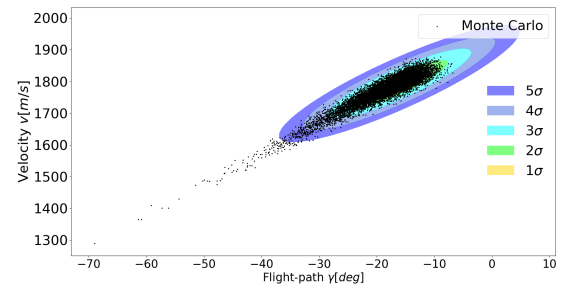
(e)  $h$  vs.  $v$  at time  $t_3$



(f)  $v$  vs.  $\gamma$  at time  $t_3$

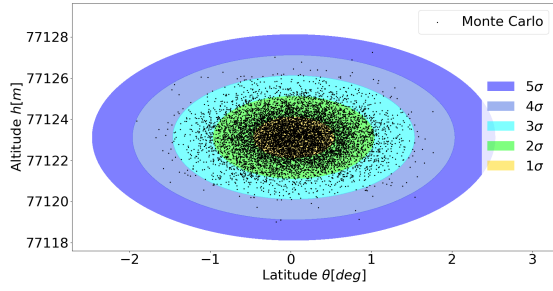


(g)  $h$  vs.  $v$  at time  $t_4$

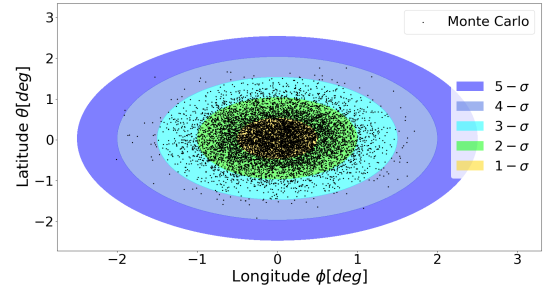


(h)  $v$  vs.  $\gamma$  at time  $t_4$

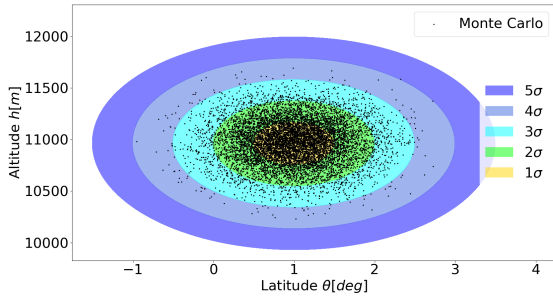
**Figure 10. Variation of altitude vs. velocity & velocity vs. flight-path at different time-steps**



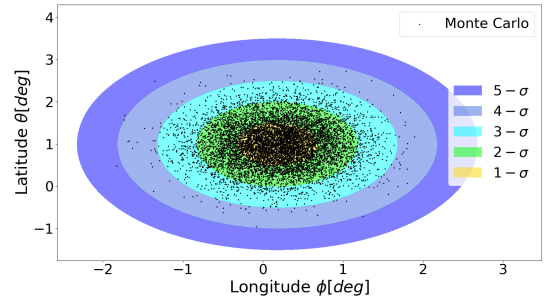
(a)  $h$  vs.  $\theta$  at time  $t_1$



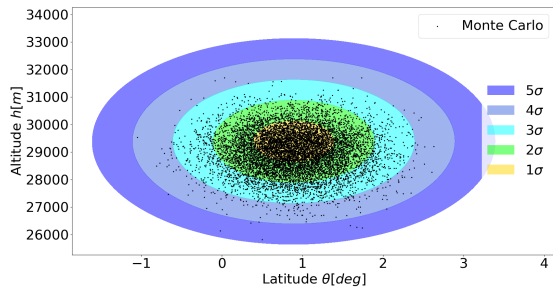
(b)  $\theta$  vs.  $\phi$  at time  $t_1$



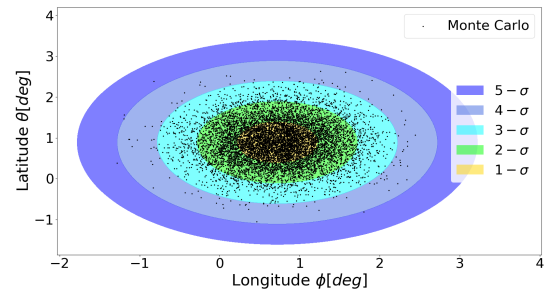
(c)  $h$  vs.  $\theta$  at time  $t_2$



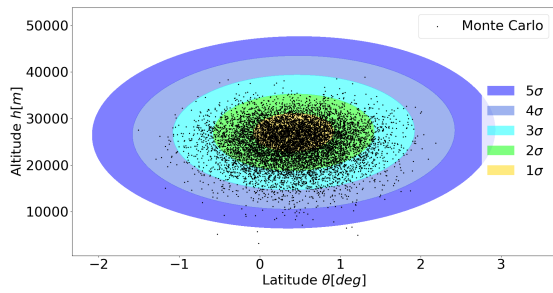
(d)  $\theta$  vs.  $\phi$  at time  $t_2$



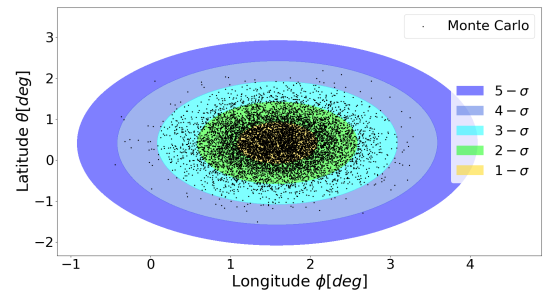
(e)  $h$  vs.  $\theta$  at time  $t_3$



(f)  $\theta$  vs.  $\phi$  at time  $t_3$

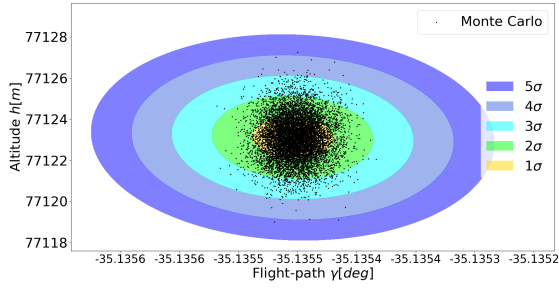


(g)  $h$  vs.  $\theta$  at time  $t_4$

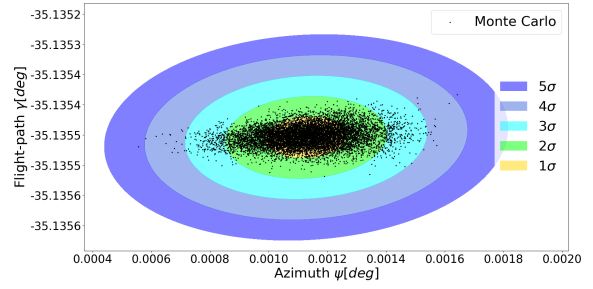


(h)  $\theta$  vs.  $\phi$  at time  $t_4$

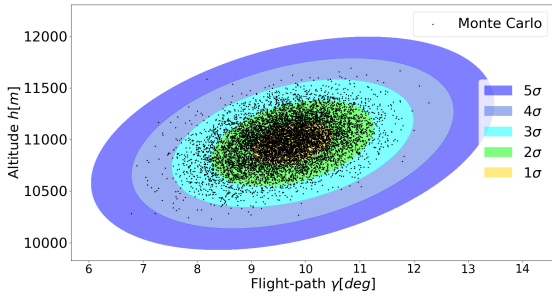
**Figure 11. Variation of altitude vs. latitude & latitude vs. longitude at different time-steps**



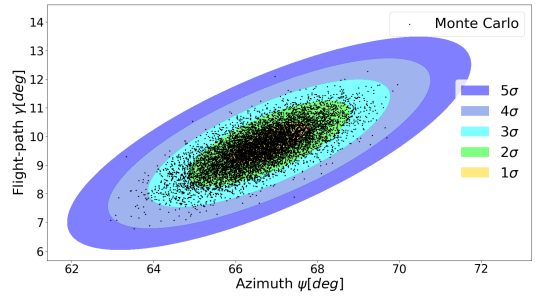
(a)  $h$  vs.  $\gamma$  at time  $t_1$



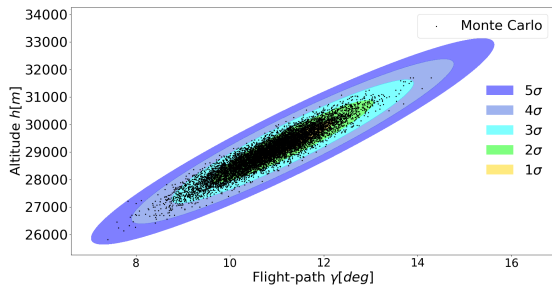
(b)  $\gamma$  vs.  $\psi$  at time  $t_1$



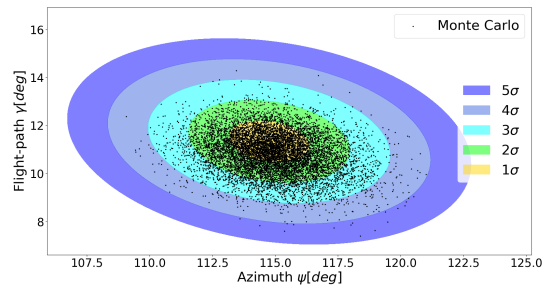
(c)  $h$  vs.  $\gamma$  at time  $t_2$



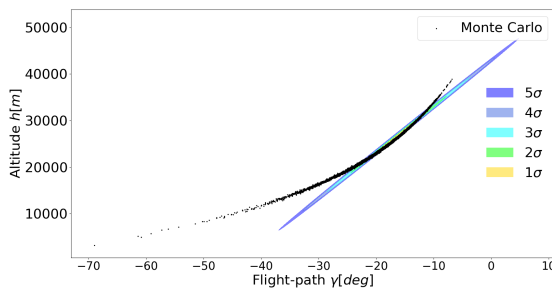
(d)  $\gamma$  vs.  $\psi$  at time  $t_2$



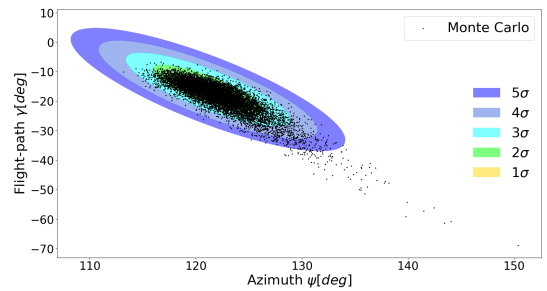
(e)  $h$  vs.  $\gamma$  at time  $t_3$



(f)  $\gamma$  vs.  $\psi$  at time  $t_3$



(g)  $h$  vs.  $\gamma$  at time  $t_4$



(h)  $\gamma$  vs.  $\psi$  at time  $t_4$

**Figure 12. Variation of altitude vs. flight-path & flight-path vs. azimuth at different time-steps**

## CONCLUSIONS

A computationally efficient probabilistic approach has been presented to compute reachability sets for a generic nonlinear system. The developed approach exploits the independence of state variable and control input variable to curtail the conventional combinatorial growth of samples associated with computation of reachability sets. Furthermore, Conjugate Unscented Transformation (CUT) is used to compute multi-dimensional expectation integrals required to compute desired order moments associated with state density function at each time. Two different optimal maneuvers associated with hypersonic reentry problem are considered to show the efficacy of the developed approach. Numerical experiments presented in the paper clearly demonstrate the ability of the developed approach in accurately approximating the reachability sets and provide a basis for optimism in developed approach. The main advantage of the developed approach is that it provides a tradeoff between computations and accuracy in approximating reachability sets by controlling the number of statistical moments to be computed.

## ACKNOWLEDGEMENT

This material is based upon work supported through National Science Foundation (NSF) under Awards No. CMMI- 1826990.

## APPENDIX

The third order moments can be computed as:

$$\mathbb{E} \left[ x_{k+1}^\alpha x_{k+1}^\beta x_{k+1}^\gamma \right] = \mathbb{E} \left[ (f^\alpha(\mathbf{x}_k) + G^{\alpha a}(\mathbf{x}_k) h^a(\mathbf{u}_k))^3 \right] \quad (28)$$

$$\begin{aligned} &= \mathbb{E} \left[ f^\alpha(\mathbf{x}_k) f^\beta(\mathbf{x}_k) f^\gamma(\mathbf{x}_k) \right] + \mathbb{E} \left[ f^\alpha(\mathbf{x}_k) f^\beta(\mathbf{x}_k) G^{\gamma c}(\mathbf{x}_k) h^c(\mathbf{u}_k) \right] \\ &+ \mathbb{E} \left[ f^\alpha(\mathbf{x}_k) G^{\beta b}(\mathbf{x}_k) h^b(\mathbf{u}_k) f^\gamma(\mathbf{x}_k) \right] + \mathbb{E} \left[ f^\alpha(\mathbf{x}_k) G^{\beta b}(\mathbf{x}_k) h^b(\mathbf{u}_k) G^{\gamma c}(\mathbf{x}_k) h^c(\mathbf{u}_k) \right] \\ &+ \mathbb{E} \left[ G^{\alpha a}(\mathbf{x}_k) h^a(\mathbf{u}_k) f^\beta(\mathbf{x}_k) f^\gamma(\mathbf{x}_k) \right] + \mathbb{E} \left[ G^{\alpha a}(\mathbf{x}_k) h^a(\mathbf{u}_k) f^\beta(\mathbf{x}_k) G^{\gamma c}(\mathbf{x}_k) h^c(\mathbf{u}_k) \right] \\ &+ \mathbb{E} \left[ G^{\alpha a}(\mathbf{x}_k) h^a(\mathbf{u}_k) G^{\beta b}(\mathbf{x}_k) h^b(\mathbf{u}_k) f^\gamma(\mathbf{x}_k) \right] \\ &+ \mathbb{E} \left[ G^{\alpha a}(\mathbf{x}_k) h^a(\mathbf{u}_k) G^{\beta b}(\mathbf{x}_k) h^b(\mathbf{u}_k) G^{\gamma c}(\mathbf{x}_k) h^c(\mathbf{u}_k) \right] \\ &\alpha, \beta, \gamma = 1, 2, \dots, n, \quad a, b, c = 1, 2, \dots, r \end{aligned} \quad (29)$$

Again, making use of the fact that  $\mathbf{x}_k$  is independent of  $\mathbf{u}_k$ , the aforementioned expression can be simplified as follows:

$$\begin{aligned}
\mathbb{E} \left[ x_{k+1}^\alpha x_{k+1}^\beta x_{k+1}^\gamma \right] &= \mathbb{E} \left[ f^\alpha(\mathbf{x}_k) f^\beta(\mathbf{x}_k) f^\gamma(\mathbf{x}_k) \right] + \mathbb{E} \left[ f^\alpha(\mathbf{x}_k) f^\beta(\mathbf{x}_k) G^{\gamma c}(\mathbf{x}_k) \right] \mathbb{E} [h^c(\mathbf{u}_k)] \\
&+ \mathbb{E} \left[ f^\alpha(\mathbf{x}_k) G^{\beta b}(\mathbf{x}_k) f^\gamma(\mathbf{x}_k) \right] \mathbb{E} [h^b(\mathbf{u}_k)] \\
&+ \mathbb{E} \left[ f^\alpha(\mathbf{x}_k) G^{\beta b}(\mathbf{x}_k) G^{\gamma c}(\mathbf{x}_k) \right] \mathbb{E} [h^b(\mathbf{u}_k) h^c(\mathbf{u}_k)] \\
&+ \mathbb{E} \left[ G^{\alpha a}(\mathbf{x}_k) f^\beta(\mathbf{x}_k) f^\gamma(\mathbf{x}_k) \right] \mathbb{E} [h^a(\mathbf{u}_k)] \\
&+ \mathbb{E} \left[ G^{\alpha a}(\mathbf{x}_k) f^\beta(\mathbf{x}_k) G^{\gamma c}(\mathbf{x}_k) \right] \mathbb{E} [h^a(\mathbf{u}_k) h^c(\mathbf{u}_k)] \\
&+ \mathbb{E} \left[ G^{\alpha a}(\mathbf{x}_k) G^{\beta b}(\mathbf{x}_k) f^\gamma(\mathbf{x}_k) \right] \mathbb{E} [h^a(\mathbf{u}_k) h^b(\mathbf{u}_k)] \\
&+ \mathbb{E} \left[ G^{\alpha a}(\mathbf{x}_k) G^{\beta b}(\mathbf{x}_k) G^{\gamma c}(\mathbf{x}_k) \right] \mathbb{E} [h^a(\mathbf{u}_k) h^b(\mathbf{u}_k) h^c(\mathbf{u}_k)]
\end{aligned} \tag{30}$$

## REFERENCES

- [1] T. A. Henzinger, P. H. Ho, and H. W. Toi. *TACAS 95: Tools and algorithms for the construction and analysis of systems, Lecture Notes in Computer Science*, volume 1019, chapter A user guide to HYTECH, pages 41–71. Springer, 1995.
- [2] O. Botchkarev and S. Tripakis. *Hybrid systems: Computation and control, Lecture Notes in Computer Science*, volume 1790, chapter Verification of hybrid systems with linear differential inclusions using ellipsoidal approximations, pages 73–88. Springer, 2000.
- [3] A. Chutinan and B. Krogh. *Hybrid systems: Computation and control, Lecture Notes in Computer Science*, volume 1569, chapter Verification of polyhedral-invariant hybrid automata using polygonal flow pipe approximations, pages 76–90. Springer, 1999.
- [4] M. Greenstreet and I. Mitchell. *Hybrid systems: Computation and control, Lecture Notes in Computer Science*, volume 1386, chapter Integrating projections, pages 159–171. Springer, 1998.
- [5] A. Kurzanski and P. Varaiya. *Hybrid systems: Computation and control, Lecture Notes in Computer Science*, volume 1790, chapter Ellipsoidal techniques for reachability analysis, pages 202–214. Springer, 2000.
- [6] I. Mitchell and C. Tomlin. *Hybrid systems: Computation and control, Lecture Notes in Computer Science*, volume 1790, chapter Level set methods for computation in hybrid systems, pages 310–323. Springer, 2000.
- [7] Jung Soon Jang and Claire Tomlin. Control strategies in multi-player pursuit and evasion game. In *AIAA Guidance, Navigation, and Control Conference and Exhibit*, page 6239, 2005.
- [8] J. Lygeros. On reachability and minimum cost optimal control. *Automatica*, 40(6):917–927, 2004.
- [9] J. Löfberg. Yalmip : A toolbox for modeling and optimization in matlab. In *In Proceedings of the CACSD Conference*, Taipei, Taiwan, 2004.
- [10] J. Löfberg. Pre- and post-processing sum-of-squares programs in practice. *IEEE Transactions on Automatic Control*, 54(5):1007–1011, 2009.
- [11] Ian M. Mitchell and Jeremy A. Templeton. *Lecture Notes in Computer Science (LNCS) 3414: Hybrid Systems Computation and Control*, chapter A Toolbox of Hamilton-Jacobi Solvers for Analysis of Nondeterministic Continuous and Hybrid Systems, pages 480–494. Springer-Verlag, March 2005.
- [12] J. Lygeros. Minimum Cost Optimal Control: An Application to Flight Level Tracking. In *Mediterranean on Control and Automation*, Rhodes, Greece., June 2003.
- [13] I. Kitsios and J. Lygeros. Launch-pad Abort Flight Envelope Computation for a Personnel Launch Vehicle Using Reachability. In *AIAA Guidance, Navigation and Control Conference and Exhibit*, San Francisco, California, USA, August 2005.
- [14] I. Kitsios and J. Lygeros. Aerodynamic Envelope Computation for Safe Landing of the HL-20 Personnel Launch Vehicle using Hybrid Control. In *Mediterranean on Control and Automation*, Nicosia, Cyprus., June 2005.

- [15] Anirudha Majumdar, Ram Vasudevan, Mark M Tobenkin, and Russ Tedrake. Convex optimization of nonlinear feedback controllers via occupation measures. *The International Journal of Robotics Research*, 2014.
- [16] R. Tedrake, I. R. Manchester, M. M. Tobenkin, and J. W. Roberts. Lqr-trees: Feedback motion planning via sums of squares verification. *International Journal of Robotics Research*, 29:1038–1052, 2010.
- [17] Marcus J Holzinger and Daniel J Scheeres. Reachability results for nonlinear systems with ellipsoidal initial sets. *IEEE transactions on aerospace and electronic systems*, 48(2):1583–1600, 2012.
- [18] Ross E Allen, Ashley A Clark, Joseph A Starek, and Marco Pavone. A machine learning approach for real-time reachability analysis. In *Intelligent Robots and Systems (IROS 2014), 2014 IEEE/RSJ International Conference on*, pages 2202–2208. IEEE, 2014.
- [19] Erik Komendera, Elizabeth Bradley, and Daniel Scheeres. Efficiently locating impact and escape scenarios in spacecraft reachability sets. In *AIAA/AAS Astrodynamics Specialist Conference*, page 4810, 2012.
- [20] N. Adurthi and P. Singla. A conjugate unscented transformation based approach for accurate conjunction analysis. *AIAA Journal of Guidance, Control and Dynamics*, 38(9):1642–1658, Sep. 2015.
- [21] Pablo A. Parrilo. *Structured Semidefinite Programs and Semialgebraic Geometry Methods in Robustness and Optimization*. PhD thesis, California Institute of Technology, May 2000.
- [22] Thomas Gerstner and Michael Griebel. Numerical integration using sparse grids. *Numerical Algorithms*, 18:209–232, 1998. 10.1023/A:1019129717644.
- [23] A. H. Stroud and D. Secrest. *Gaussian Quadrature Formulas*. Englewood Cliffs, NJ: Prentice Hall, 1966.
- [24] N. Adurthi, P. Singla, and T. Singh. The conjugate unscented transform-an approach to evaluate multi-dimensional expectation integrals. Proceedings of the American Control Conference, June 2012.
- [25] Nagavenkat Adurthi, Puneet Singla, and Tarunraj Singh. Conjugate unscented transformation: Applications to estimation and control. *Journal of Dynamic Systems, Measurement, and Control*, 140(3):030907, 2018.
- [26] N. Adurthi. The conjugate unscented transform - a method to evaluate multidimensional expectation integrals. Master’s thesis, University at Buffalo, 2013.
- [27] N. Adurthi, P. Singla, and T. Singh. Conjugate unscented transform rules for uniform probability density functions. Proceedings of the American Control Conference, June 2013.
- [28] N. Adurthi, P. Singla, and T. Singh. Conjugate unscented transform and its application to filtering and stochastic integral calculation. AIAA Guidance, Navigation, and Control Conference, August 2012.
- [29] Marcus Bursik, Matthew Jones, Simon Carn, Ken Dean, Abani Patra, Michael Pavolonis, E. Bruce Pitman, Tarunraj Singh, Puneet Singla, Peter Webley, Halldor Bjornsson, and Maurizio Ripepe. Estimation and propagation of volcanic source parameter uncertainty in an ash transport and dispersal model: Application to the Eyjafjallajokull plume of 14–16 April 2010. *Bulletin of Volcanology*, 74(10):2321–2338, 2012.
- [30] R. Madankan, S. Pouget, P. Singla, M. Bursik, J. Dehn, M. Jones, A. Patra, M. Pavolonis, E. B. Pitman, T. Singh, and P. Webley. Computation of probabilistic hazard maps and source parameter estimation for volcanic ash transport and dispersion. *Journal of Computational Physics*, 271:39–59, 2014.
- [31] N. Adurthi, P. Singla, and M. Majji. Conjugate unscented transform based approach for dynamic sensor tasking and space situational awareness. In *American Control Conference (ACC), 2015*, pages 5218–5223. IEEE, 2015.
- [32] R. Madankan, P. Singla, T. Singh, and P. D. Scott. Polynomial chaos based Bayesian approach for state and parameter estimation. *AIAA Journal of Guidance, Navigation, and Control*, 36(4):1058–1074, 2013.
- [33] Knut Graichen and Nicolas Petit. Constructive methods for initialization and handling mixed state-input constraints in optimal control. *Journal Of Guidance, Control, and Dynamics*, 31(5):1334–1343, 2008.
- [34] Justin R Mansell and Michael J Grant. Adaptive continuation strategy for indirect hypersonic trajectory optimization. *Journal of Spacecraft and Rockets*, 55(4):818–828, 2018.
- [35] Amy F Woolf. Conventional prompt global strike and long range ballistic missiles: Background and issues. Technical report, Congressional Research Service Washington United States, 2017.